Hindawi
Advances in Materials Science and Engineering
Volume 2017, Article ID 5386498, 10 pages
https://doi.org/10.1155/2017/5386498

Research Article

Numerical Simulation of GFRP Reinforced Concrete Beams

Xia Zhao,[1,2] Xiong-Jun He,[1] and Yong-Chao Yang[1]

[1]*School of Transportation, Wuhan University of Technology, Wuhan, Hubei 430063, China*
[2]*Binzhou Polytechnic, Binzhou, Shandong 256603, China*

Correspondence should be addressed to Xia Zhao; yxzhaoxia@sina.com

Received 22 April 2017; Accepted 19 July 2017; Published 24 August 2017

Academic Editor: Fabrizio Sarasini

Experiment on the constitutive model of fiber reinforced concrete with volume fraction of alkali-resistant glass fiber of, respectively, 0.0%, 0.5%, 1.0%, and 1.5% was conducted, and the constitutive relation of tension stress-strain full curve of GFRC shaft was obtained; the constitutive relation of GFRP is obtained by experiment, and the secant modulus was obtained by the fitting of univariate cubic equation. The finite element numerical simulation of GFRP fiber reinforced concrete beam was carried out, and the load deflection nephogram of fiber reinforced concrete beam, strain nephogram, crack nephogram, and GFRP stress nephogram were obtained. When the fiber content is 1.0%, the bearing capacity of GFRP reinforced concrete beams is the best, and it could play a "bridging" effect when the incorporation of fiber is within the load range of about 60%, which inhibited the developing speed of cracks, but with the gradual increase of the load, the "bridging" effect disappeared.

1. Introduction

In bridge engineering, the problem of steel bar corrosion has increasingly affected the use of bridges, and the emergence of new composite materials provides an effective way for solving the problem of steel bar corrosion, that is, to replace or partly replace steel bar with new composite materials. There are many varieties of fiber composite materials, mainly including SFRP (Steel Fiber Reinforced Polymer), GFRP (Glass Fiber Reinforced Polymer), CFRP (Carbon Fiber Reinforced Polymer), and AFRP (Aramid Fiber Reinforced Polymer), among which GFRP is cheaper. The GFRP beam produced by totally replacing or partly replacing steel bar with new composite materials has become a powerful trend in the future development of structures. The incorporation of fiber can not only effectively improve the brittle failure of concrete, but also effectively control the size and development of crack defects, thus ultimately improving the mechanical properties and durability of concrete structures [1–8]. Domestic and foreign researchers [9–18] adopted various finite element software to simulate CFRP reinforced prestressed concrete beam, BFRP reinforced concrete beam, and GFRP reinforced concrete beam and to simulate the variation trends such as load, deflection, crack, and bond slip, so as to make comparative analysis with the test results and obtain relevant difference conclusions.

The alkali-resistant glass fiber was incorporated into the concrete to form GFRC (Glass Fiber Reinforced Concrete). The numerical simulation of four-point bending test of GFRP reinforced concrete beams with 0.0%, 0.5%, 1.0%, and 1.5% fiber volume incorporation was carried out to obtain the bearing capacity, which was compared with the calculated test values to analyze the influence of the fiber incorporation amount on the bearing capacity of GFRP reinforced concrete beam.

2. Experiment Section

2.1. Basic Properties of Raw Materials of the Test. The experimental cement is the ordinary silicate cement with strength grade of 42.5 produced by Binzhou Qinglongshan Cement Plant, with fineness modulus of the experimental sand of 2.9, apparent density of 2710 kg/m^3, bulk density of 1600 kg/m^3, bulk density porosity of 45%, and stone powder content of 5.1%. The experimental stone is the ordinary concrete-used crushed stone produced in Qingzhou, Shandong, with apparent density of 2700 kg/m^3, bulk density of 1420 kg/m^3,

Table 1: Alkali-resistant glass fiber characteristics parameters.

Length/mm	Length-to-diameter ratio	Original wire diameter/μm	Ignition loss LO/%	Moisture content MOL/%
36	58	14–19	0.80–2.00	≤0.50

Table 2: Mechanical parameters of GFRP bar.

Diameter/mm	Density/kg·m^{-3}	Extreme tensile strength/kN	Tensile strength/MPa	Elastic modulus/GPa
10	2200	72	980	42

Table 3: Fiber-concrete incorporation ratio design.

Number	Cement/kg	Coarse aggregate/kg	River sand/kg	Water/kg	Water-reducer/kg·m^{-3}	Fibers/vol.%
1#	500	1045	700	200	3.0	0
2#	500	1045	700	200	3.0	0.5
3#	500	1045	700	200	3.0	1.0
4#	500	1045	700	200	3.0	1.5

Table 4: Test data of the axial compressive strength of fiber reinforced concrete.

Fiber incorporation/%	Compressive area A/mm^2	Ultimate load F/kN	Compressive strength f_{cu}/MPa
0.0	10000	48.30	48.30
0.5	10000	52.22	52.22
1.0	10000	46.50	46.50
1.5	10000	42.68	42.68

crushing index of 9.9%, mud content of 0.5%, bulk density porosity of 47%, and needle-like particle content of 4%. The experimental water-reducing agent is the FMY-1 water-reducing agent produced by Binzhou Meiya Building Materials Technology Co., Ltd. The experiment water is tap water.

The experimental glass fiber is the alkali-resistant glass fiber specially used for bridge concrete provided by Taishan Fiberglass Co., Ltd., and the characteristic parameters are shown in Table 1.

In the table, the original wire diameter conforms to the standard of ISO1888: 2006, the ignition loss conforms to the standard of ISO1887: 1995, and the water content conforms to the standard of ISO 3344: 1997. The fiber has high zirconium content and conforms to the standards of ASTM C1666/C 1666/M-07 and EN15422, and according to PCI and GRCA, it is suggested for production. GFRP bar is provided by Nanjing Fenghui Composite Materials Co., Ltd., with diameter of 10 mm and length of 1100 mm. The mechanical properties of the experimental glass fiber bar are shown in Table 2.

2.2. Fiber Concrete Incorporation Ratio Design. According to the literature [19], the incorporation ratio of the glass fiber reinforced concrete is designed in accordance with the cement, sand, stone, and water ratio of 1 : 1.40 : 2.09 : 0.40, and the incorporation amount of water-reducing agent is 3.0 kg/cubic concrete; the fiber volume incorporation contents were, respectively, 0.0%, 0.5%, 1.0%, and 1.5%, and the incorporation ratio is shown in Table 3.

2.3. Specimen Design. The cross-section design size of the experimental beam is 80 mm × 110 mm; the length is 1100 mm, and the thickness of the protective layer of GFRP is 30 mm, as shown in Figure 1. The incorporation of alkali-resistant glass fiber distributed randomly in the concrete.

3. Numerical Simulation

The numerical simulation was carried out by ABAQUS finite element software, and the choice of parameters in the software simulation had great effect on the simulation results. Since there are a variety of constitutive models, and the calculation of nonlinear model has heavy workload, now there are no literatures that have made comparison and analysis on the differences between the various models. Therefore, in order to reflect the actual force process of GFRP reinforced concrete beams as much as possible, the methods of experimental research and theoretical analysis were used to analyze the constitutive model of fiber reinforced concrete in this numerical model.

3.1. Constitutive Model of GFRC Axial Compression Experiment. Axial compression experiments were, respectively, carried out on cubic fiber reinforced concrete with fiber incorporation of 0.0%, 0.5%, 1.0%, and 1.5%, and the YAW-2000B microcomputer controlled electrohydraulic pressure experimenting machine was used as the experimental equipment. The experimental data of axial compressive strength and fiber incorporation are shown in Table 4. According

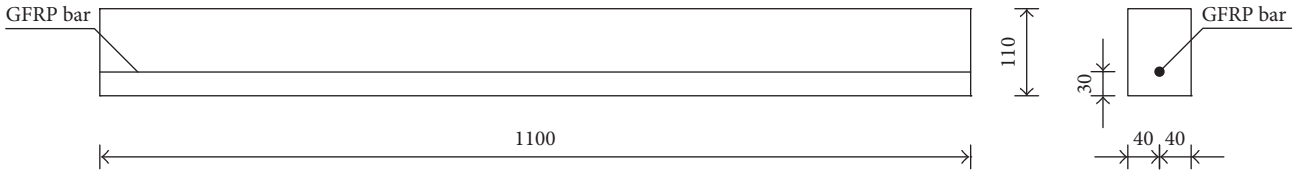

Figure 1: Design figure of GFRP reinforced fiber reinforced concrete beam (unit: mm).

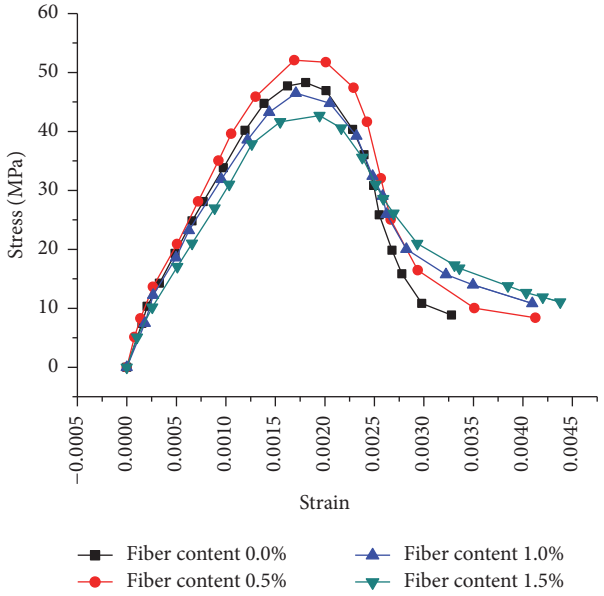

Figure 2: Stress-strain curves of fiber reinforced concrete under uniaxial compression.

Figure 3: Splitting tensile strength test in [20].

to the axial compressive strength of fiber concrete, it can be concluded that when the fiber incorporation amount is 0.5%, the axial compressive strength is the best, and with the increase of fiber incorporation, the axial compressive strength is decreased.

The constitutive model of the compressive stress-strain curve corresponding to the four types of fiber reinforced concrete with different fiber incorporation was sketched according to the data obtained in the experiment, as shown in Figure 2.

3.2. Constitutive Model of GFRC Axial Tensile Test. The numerical simulation of the axial tension of steel reinforced concrete was carried out, and the parameters equation given by Zhenhai and Xudong [21] and common concrete tensile model were mostly adopted, that is, the uniaxial tensile stress-strain curve equation of glass fiber reinforced concrete. Domestic and foreign scholars have not given definite parametric equation, and [20, 22, 23] give the constitutive curve of the fiber reinforced concrete experiment. In light of the experimental conditions of this study and the personal ability, the axial tension full curve of fiber reinforced concrete was obtained in segments: in the ascending segment, the experiment method was used, and the descending segment was in accordance with [20, 22, 23]. From the theoretical analysis on the descending segment of the axial tensile stress-strain full curve of GFRP fiber reinforced concrete, that is, according to "Experimental Method Standard for Mechanical Properties of Common Concrete" (GB/T 50081-2002), the splitting tensile strength of fiber reinforced concrete was obtained by 100 mm cubic splitting tensile experiment. After converting it into concrete axial tensile strength, the ascending segment of the axial tensile stress-strain full curve of fiber reinforced concrete was obtained, with the formula shown in

$$f_{ts} = \frac{2F}{\pi A} = 0.637\frac{F}{A}, \tag{1}$$

where f_{ts} is the splitting tensile strength of concrete, unit: MPa; the calculation is accurate to 0.01 MPa; F is the failure load of the specimen, unit N; A is the specimen splitting area, unit: mm^2.

The cylinder splitting experiment in [20] was conducted according to the ASTM C 496/C496-2004 standard, as seen in Figure 3. WAW-300/WAW-1000 microcomputer controlled electrohydraulic servo universal experimenting machine was used in this experiment, and the comparison of the fiber reinforced concrete specimen before and after the splitting experiment is shown in Figure 4. The peak strain of the concrete was calculated by using (3), and the tensile elasticity modulus was calculated by using (4). The splitting tensile experiment data are shown in Table 5.

$$f_t = 0.9 f_{ts} \tag{2}$$

$$\varepsilon_{tp} = 65 \times 10^{-6} f_t^{0.54} \tag{3}$$

$$E_t = (1.45 + 0.628 f_t) \times 10^4. \tag{4}$$

Table 5: Splitting tensile strength test data of fiber reinforced concrete.

Fiber incorporation amount/%	Splitting area A/mm^2	Ultimate load F/k N	Nonstandard splitting tensile strength/MPa	Conversion coefficient k	Splitting tensile strength f_{ts}/MPa	Axial tensile strength f_t/MPa	Axial tensile peak strain ε_{tp}/%	Axial tensile elasticity modulus E_t/K Pa	Peak secant modulus E_{tp}/K Pa	E_t/E_{tp}
0.0	10000	22.91	2.291	0.85	1.9474	1.753	0.8801	25.51	19.92	1.28
0.5	10000	25.13	2.413	0.85	2.0511	1.846	0.9051	26.09	20.40	1.28
1.0	10000	24.96	2.496	0.85	2.1216	1.909	0.9216	26.48	20.72	1.28
1.5	10000	21.66	2.166	0.85	1.8411	1.657	0.8537	24.91	19.41	1.28

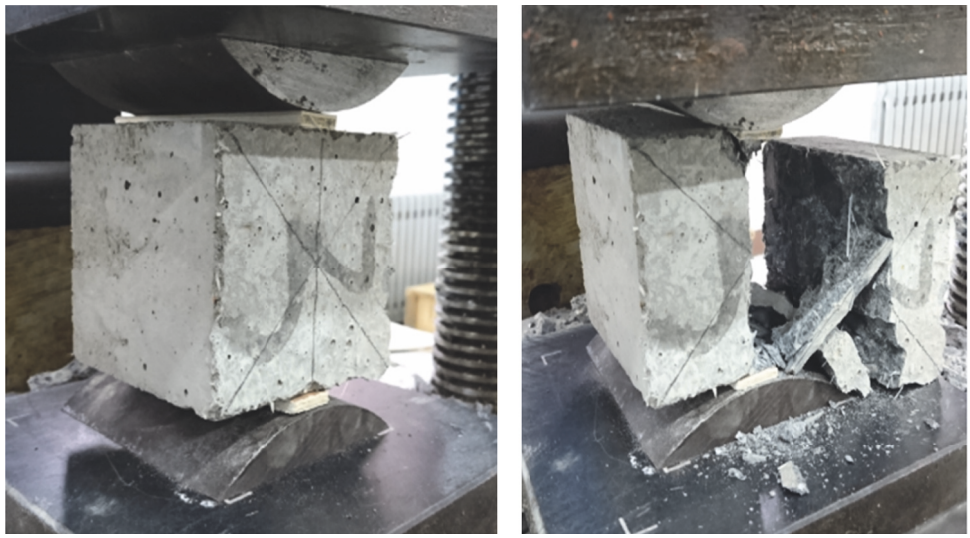

Figure 4: Splitting tensile strength test in this experiment.

E_t/E_{tp} = 1.28, which is in accordance with the ratio proposed by Professor Guo Zhenhai, that is, within the range between 1.04 and 1.38. Generally, it is taken as 1.20, and the data obtained in this experiment is 1.28, which is within the normal ratio range and verifies the reliability of the data.

The ascending segment of the axial tensile stress-strain full curve was obtained according to the splitting tensile test data, and the descending segment of the axial tensile stress-strain full curve was obtained according to the tensile stress-strain typical curve of alkali-resistant glass fiber reinforced concrete in [22, 23]. The ascending and descending segments were combined to complete the tensile stress-strain full curves of the four types of concrete with different fiber incorporation, as shown in Figure 5.

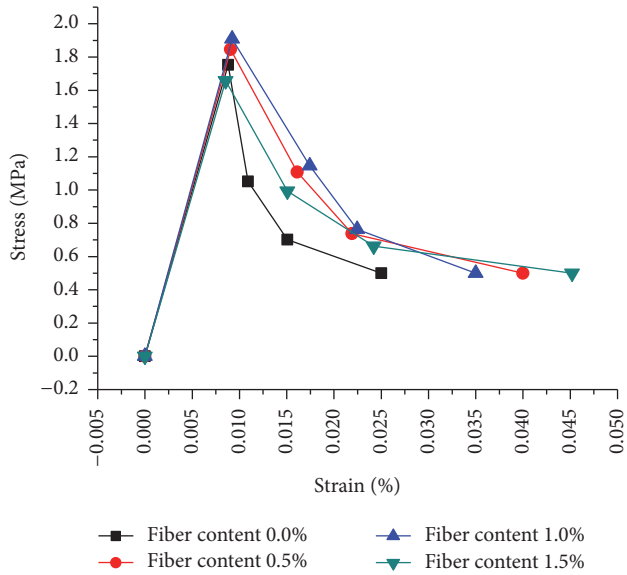

Figure 5: Axial tensile stress-strain full curve.

3.3. Constitutive Model of GFRP Test. The basic input parameters of the experimental GFRP are shown in Table 2. Through the stretching of five GFRP specimens, it was obtained that the average maximum tensile stress was 839.6 MPa, the strain was 0.0155, and the stress-strain curve was linear elastic curve, as shown in Figure 6.

3.4. Parameter Calculation of GFRC Constitutive Model. The general input of the elastic modulus parameters in the numerical simulation is secant modulus, of which the secant modulus value is usually calculated by taking the secant with work stress of $\sigma = (0.4 \sim 0.5) f_c$ in the structure using stage. The calculation was carried out by taking 0.4 times of the value, that is, $E_{c,s} = \sigma_{0.4}/\varepsilon_{0.4}$. The regression equation of the ascending segment of different contents of

Table 6: Secant modulus of fiber reinforced concrete.

Fiber incorporation/%	$f_c/10^3$ N·mm^{-2}	$\sigma_{0.4} = 0.4f_c$	Simulation $\varepsilon_{0.4}$	ε_p	$E_{c,s}$/N·mm^{-2}	Ratio to standard value
0.0	48.3	19.32	0.000480	0.0016245	40250.00	1.24
0.5	52.22	20.888	0.000484	0.001691	43157.0248	1.33
1.0	46.5	18.6	0.000482	0.001707	38589.2116	1.19
1.5	42.68	17.072	0.000517	0.001946	33021.2766	1.02

Table 7: Simulation of the four-point bending bearing capacity parameters.

Fiber content/%	Cracking load/kN	Ultimate load/kN	Cracking deflection/mm	Ultimate deflection/mm
0.0	2.16	12.88	0.1212	12.5313
0.5	2.42	13.34	0.1218	12.8191
1.0	2.52	15.34	0.1428	15.9406
1.5	2.14	13.06	0.1423	13.2718

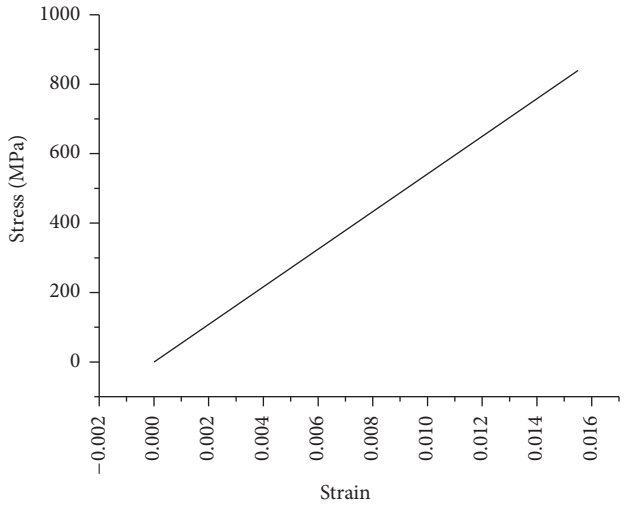

Figure 6: GFRP stress-strain constitutive model.

fiber incorporation is shown in Figure 7, in which the cubic regression curve equation was obtained by the simulation of the ascending segment of the axial compressive stress-strain curve, and it was solved to obtain the secant modulus at 0.4 times, as seen in Table 6. The Poisson's ratio of the glass fiber reinforced concrete was taken as 0.2.

3.5. Modeling Process of GFRP Reinforced Concrete Beam. Due to the symmetry of the structure, in order to simplify the calculation, the numerical simulation of the GFRP fiber reinforced concrete was analyzed by taking the semistructure. The model consists of three components, steel block, GFRP, and concrete beam. The type of the boundary condition is XSYMM, that is, symmetrical boundary condition, in which the symmetry plane is the vertical plane of the axis 1, and the limited vertical displacement of the constraint type at the support is $U2 = 0$. The load was set as the uniform load acting on the top of the steel block, and the resultant force was taken to conduct the simulation computation. The shell unit with quadrilateral mesh was used in the cushion block and the concrete beam, in which the structured mesh generation technology is used and the unit type is CPE4R. The truss unit was used in GFRP, and the type of the mesh unit is T2D2. The overall mesh generation of GFRP reinforced concrete beams is shown in Figure 8. The grid size of the concrete beam and GFRP bars is 3 mm, and the grid size of the steel cushion blocks is 5 mm.

4. Simulation Results and Evaluation of GFRP Reinforced Concrete Beam

4.1. Load Deflection Nephogram of GFRP Reinforced Fiber Concrete Beams. Through the numerical simulation of the four-point bending bearing capacity of GFRP fiber reinforced concrete beams, the key parameters such as cracking load, ultimate load, and corresponding deflection of GFRP reinforced fiber concrete beams were obtained, as seen in Table 7. It can be seen from the simulation data that fiber incorporation did not have large effect on the initial cracking load and deflection, while it had large effect on the ultimate load and deflection; when the fiber content was 1.0%, the load and deflection both reached the maximum.

4.2. Strain Nephogram of GFRP Reinforced Concrete Beams. The strain of the GFRP reinforced fiber concrete beams is seen in Figure 9, and the variation of the load value reflects the changes of the carrying capacity of the beam. When the fiber content was 1.0%, GFRP reinforced fiber concrete beam had the best bearing capacity, and as the fiber content continued increasing, the bearing capacity was decreased.

4.3. GFRP Stress Nephogram. GFRP does not have yield point, and the stresses of GFRP in the GFRP reinforced concrete beams with different amounts of fiber incorporation were obtained by numerical simulation. The maximum stress of GFRP is within the range of 360.4 MPa~369.2 MPa, which is less than the average minimum tensile stress of GFRP experiment, σ_f. This indicates that, under this condition, the failure mode of GFRP reinforced concrete beam was still the

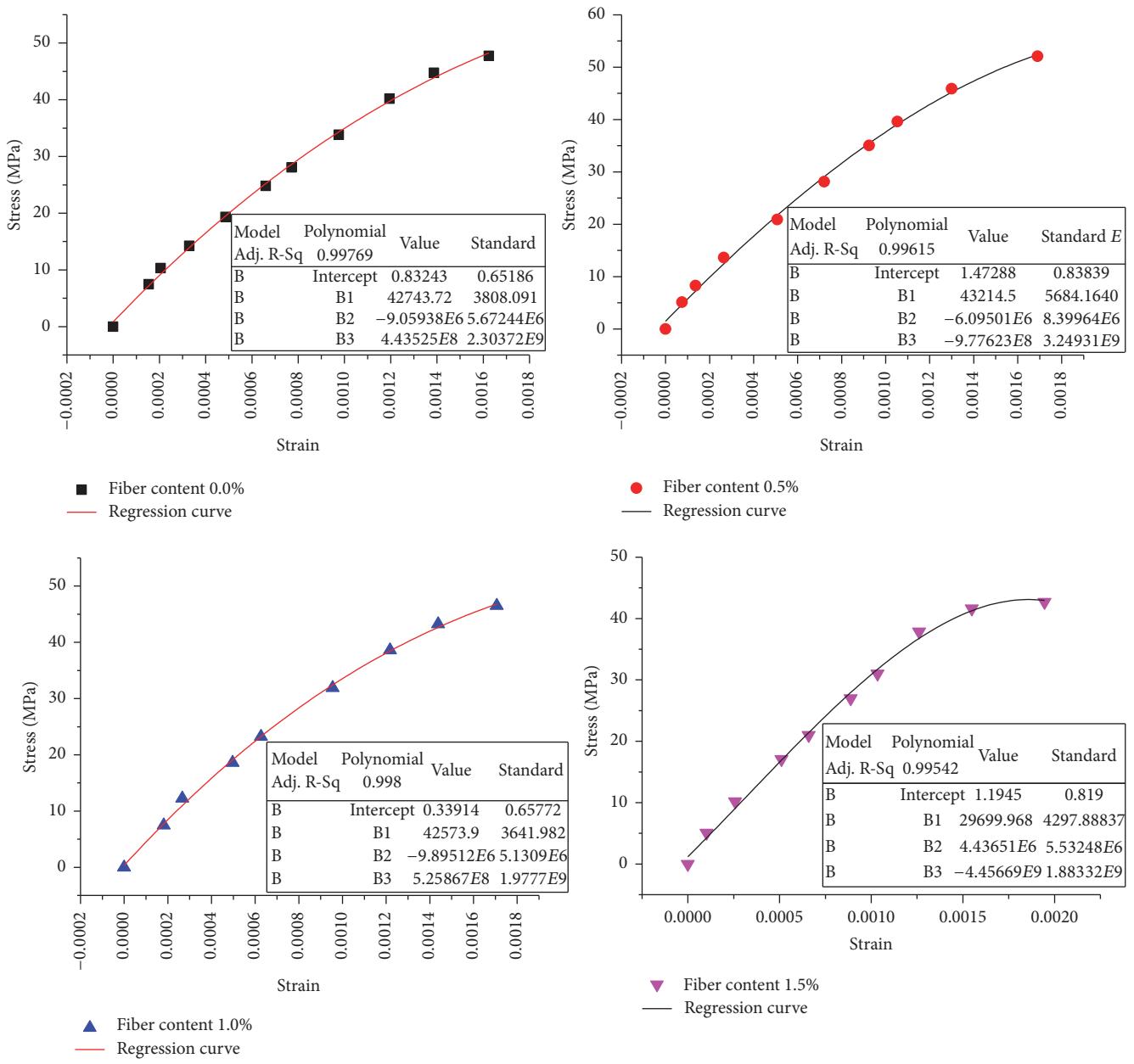

FIGURE 7: Regression curve of the compressive stress-strain ascending segment of fiber reinforced concrete.

compressive failure mode, and fiber incorporation had no effect on the stress of GFRP.

4.4. Crack Development Nephogram of GFRP Reinforced Fiber Reinforced Concrete. In this paper, the x-axis strains (LE11) corresponding to the loads of, respectively, 3 kN, 4 kN, 6 kN, 8 kN, and 12 kN were intercepted, and the trend of the x-axis strain is shown in Figure 10. The overall trend in Figure 10(a) shows that when the fiber content was 1.5%, the crack widths of the GFRP reinforced fiber concrete beams were larger than that when the fiber content was 0.0%, so the fiber content of 1.5% is undesirable. The single-point in Figure 10(b) shows that when the load is 3 kN and 4 kN, the crack widths of the GFRP reinforced fiber concrete beams, respectively, with fiber content of 0.5% and 1.0% were both less than the crack width of the GFRP reinforced concrete beam with fiber content of 0.0%. However, after loading to 6 kN, the crack width of the GFRP reinforced fiber concrete beams with fiber content of 0.5% was still less than the crack width of the GFRP reinforced fiber concrete beams with fiber content of 0.0%, while the crack width of the GFRP reinforced fiber concrete beams with fiber content of 1.0% was already greater than the crack width of the GFRP reinforced fiber concrete beams with fiber content of 0.0%. After loading to 8 kN and 12 kN, the crack widths of the GFRP reinforced fiber concrete beams with fiber content of 0.0% were all less than the crack widths of GFRP reinforced concrete beams with fiber content.

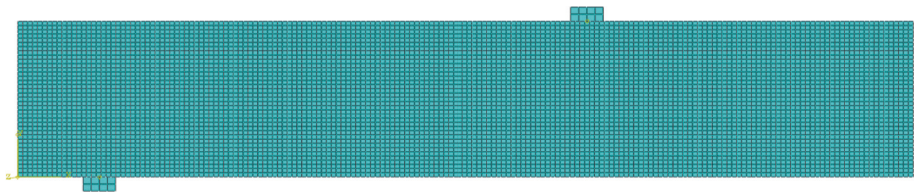

Figure 8: Mesh division of GFRP fiber reinforced concrete beam model.

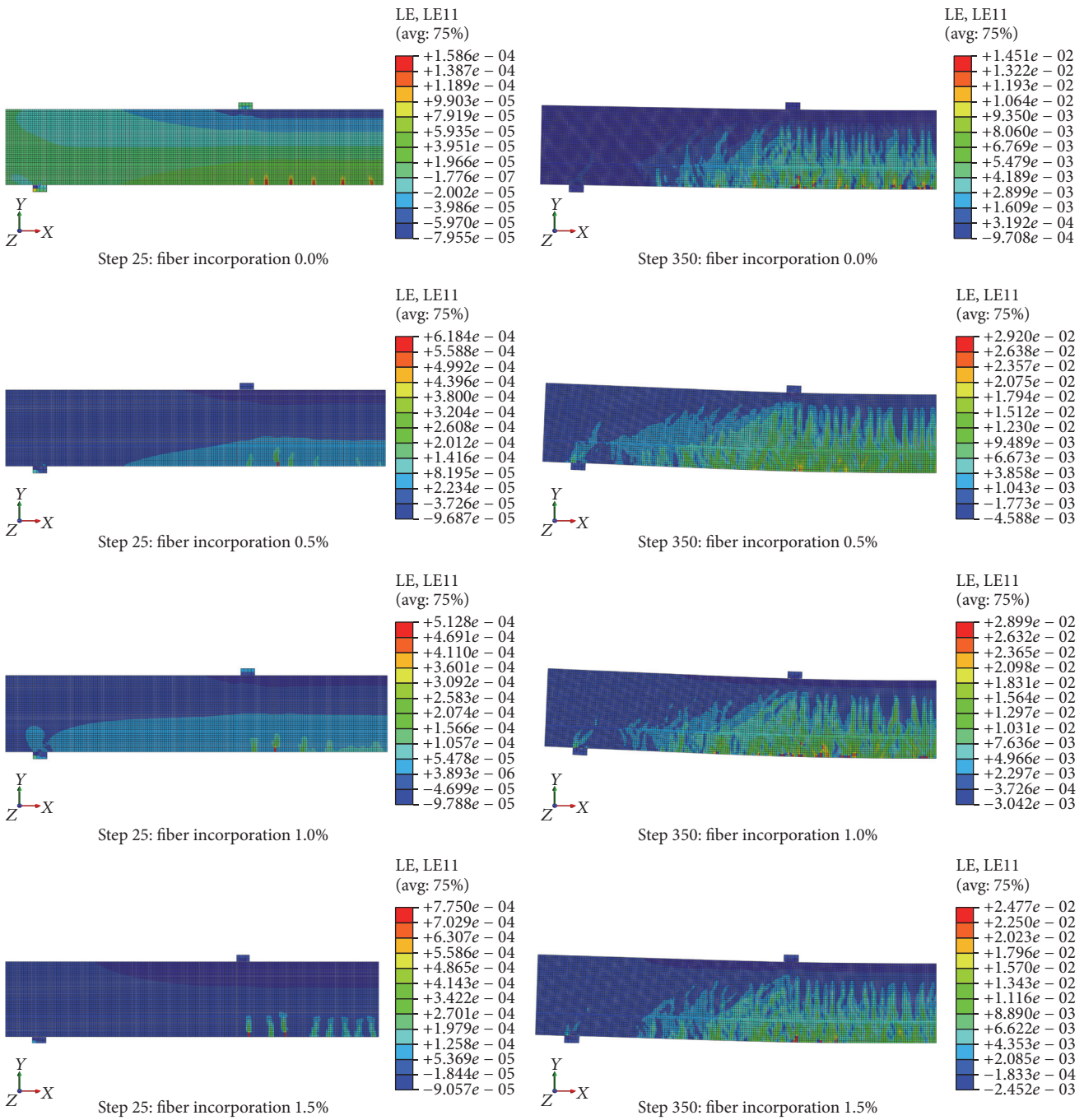

Figure 9: Strain nephogram of GFRP reinforced concrete beam.

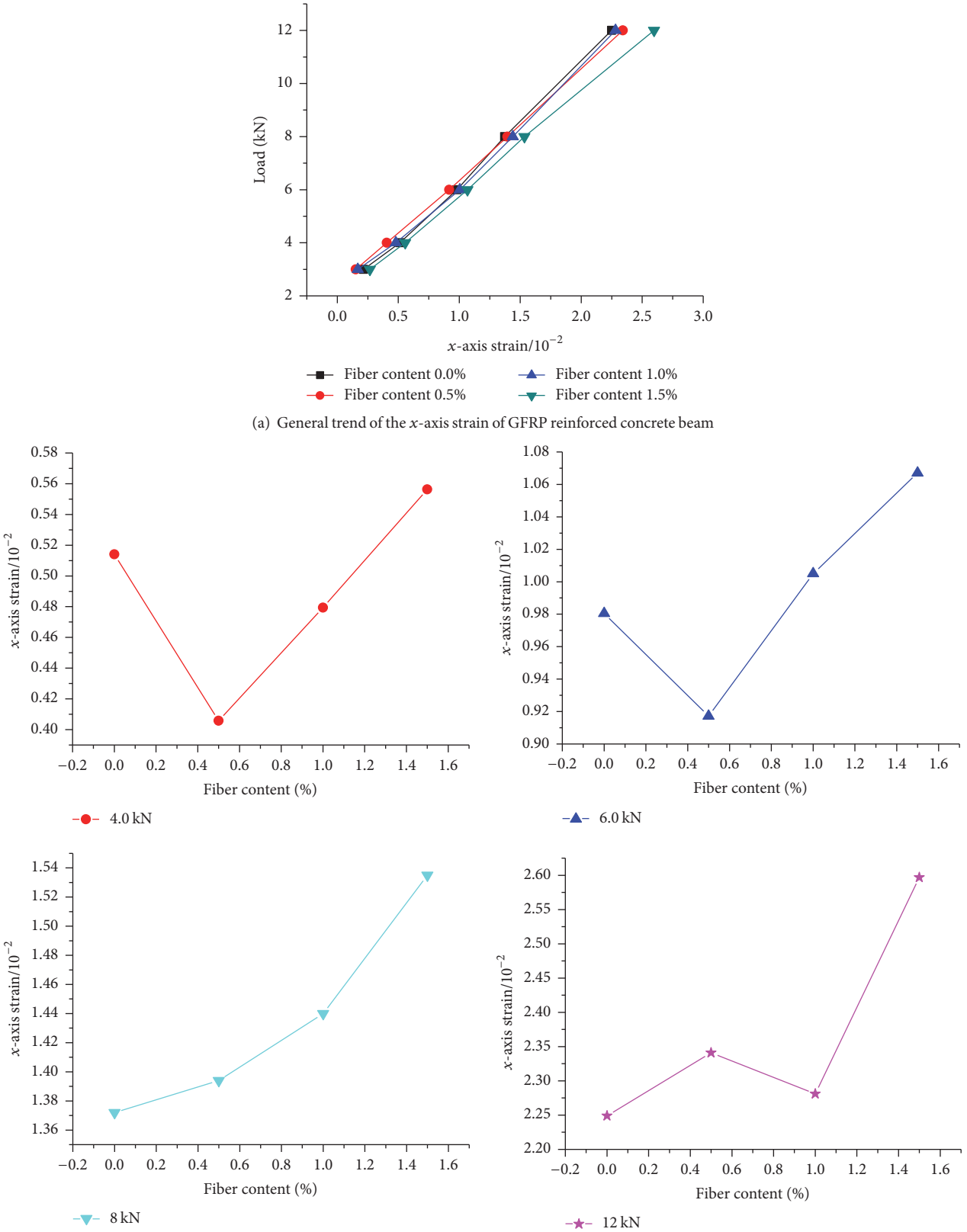

(a) General trend of the x-axis strain of GFRP reinforced concrete beam

(b) Trend of the loading point of the x-axis strain of GFRP reinforced concrete beam

Figure 10: Trend of the x-axis strain of GFRP reinforced concrete beam.

From the simulation of the bearing capacity, the glass fiber played good "bridging" effect within the load range about 60% and inhibited the development speed of the crack, but with the increase of the load, the "bridging" effect disappeared.

5. Conclusions

(1) The constitutive model of the axial compressive stress-strain curves corresponding to the four types of fiber reinforced concrete with different fiber incorporation was obtained through the axial compression experiments on cubic fiber reinforced concrete with fiber incorporation of, respectively, 0.0%, 0.5%, 1.0%, and 1.5% by using the microcomputer controlled electrohydraulic pressure experimenting machine.

(2) The constitutive model of the tensile stress-strain curve of four kinds of reinforced fiber concrete specimens with different fiber incorporation was obtained according to the splitting tensile experiment and related literature data. The constitutive model of the GFRP stress-strain full curve was obtained by experiment.

(3) Through the regression curve simulation of the ascending segment of the axial compressive stress-strain curve, the univariate cubic equation of the ascending segment was obtained, and the elastic modulus of the secant was calculated; and the finite element simulation was carried out by secant elastic modulus.

(4) Through the numerical simulation of the four-point bending bearing capacity of GFRP reinforced fiber concrete beams, the key parameters such as cracking load, ultimate load, and corresponding deflection of GFRP reinforced fiber concrete beams were obtained. Compared with GFRP reinforced concrete beams, the cracking load after fiber incorporation shows the trend of rising first and then decreasing, and the cracking load was the largest when the fiber content was 1.0%. It can be seen from the simulation data that it does not mean that it is better for GFRP reinforced fiber concrete beams to have more amount of fiber incorporation. In terms of the ultimate load, the fiber incorporation greatly increased the ultimate load of GFRP reinforced fiber concrete beams, while the ultimate load increase reached the maximum when the fiber content was 1.0%. Fiber incorporation did not have large effect on the cracking deflection, while it had large effect on ultimate deflection, and the trend is basically the same as that of the ultimate load. When the fiber content was 1.0%, the increase reached the maximum.

(5) The strain nephogram of GFRP reinforced concrete beams shows that when the concrete reached the tensile strain limit and the compression strain limit value, and the fiber content was 1.0%, the GFRP reinforced fiber concrete beams had the best bearing capacity, and as the fiber content continued increasing, the bearing capacity was decreased.

(6) The GFRP reinforced stress nephogram shows that the failure mode of GFRP reinforced fiber concrete beams was still the compressive failure mode, and fiber incorporation had no effect on the stress of GFRP.

(7) Compared with the GFRP reinforced concrete beam with no fiber incorporation, when the fiber content is 0.5% and 1.0%, it had good inhibition effect on the cracks; and when the fiber content was 1.5%, the occurrence of cracks was increased. Therefore, the fiber content of 1.5% is undesirable. From the simulation of the bearing capacity, the glass fiber played good "bridging" effect within the load range about 60% and inhibited the development speed of the crack, but with the increase of the load, the "bridging" effect disappeared.

Conflicts of Interest

The authors declare that there are no conflicts of interest regarding the publication of this paper.

Acknowledgments

The authors would like to express appreciation for the financial support by the Natural Science Foundation of China (51178361).

References

[1] S. Garcia, A. E. Naaman, and J. Pera, "Experimental investigation on the potential use of poly(vinyl alcohol) short fibers in fiber-reinforced cement-based composites," *Materials and Structures*, vol. 30, no. 195, pp. 43–52, 1997.

[2] W. Sun, H. Chen, X. Luo, and H. Qian, "The effect of hybrid fibers and expansive agent on the shrinkage and permeability of high-performance concrete," *Cement and Concrete Research*, vol. 31, no. 4, pp. 595–601, 2001.

[3] S.-H. Kwon, R. P. Ferron, Y. Akkaya, and S. P. Shah, "Cracking of fiber-reinforced self-compacting concrete due to restrained shrinkage," *International Journal of Concrete Structures and Materials*, vol. 1, no. 1, pp. 3–9, 2007.

[4] D. D. L. Chung, "Cement reinforced with short carbon fibers: a multifunctional material," *Composites Part B: Engineering*, vol. 31, no. 6-7, pp. 511–526, 2000.

[5] P.-W. Chen and D. D. L. Chung, "Carbon fiber reinforced concrete for smart structures capable of non-destructive flaw detection," *Smart Materials and Structures*, vol. 2, no. 1, pp. 22–30, 1993.

[6] S. Wen and D. D. L. Chung, "Carbon fiber-reinforced cement as a strain-sensing coating," *Cement and Concrete Research*, vol. 31, no. 4, pp. 665–667, 2001.

[7] J. C. Walraven, "High performance fiber reinforced concrete: progress in knowledge and design codes," *Materials and Structures*, vol. 42, no. 9, pp. 1247–1260, 2009.

[8] M. Hassanpour, P. Shafigh, and H. B. Mahmud, "Lightweight aggregate concrete fiber reinforcement—a review," *Construction and Building Materials*, vol. 37, pp. 452–461, 2012.

[9] X. Wei-chen, Z. Qiao-wen, and Y. Yu, "Design recommgndations on flexural capacity of FRP-reinforced concrete beam," *Engineering Mechanics*, vol. 26, no. 1, pp. 79–85, 2009.

[10] Z. Peng, *Experimental Research and Theoretical Analysis of Behavior of Concrete Beam Reinforced with FRP Bars*, Guangxi University, Nanning, Guangxi, China, 2006.

[11] J. Yang, *Experimental Study and Theoretical Analysis on Concrete Beams Reinforced with Different FRP Bars Blended*, Chongqing University, Chongqing, China, 2013.

[12] Y. Park, *Long-Term Performance of GFRP Oreinforced Conerete Beams and Barssubjected to Aggressive Environments*, The University of Texas, Arlington, Tex, USA, 2012.

[13] A. E. Naaman and S. M. Jeong, "Structural ductility of concrete beams prestressed with FRP tendons," in *Proceedings of the 2nd International RILEM Symposium, FRPRXS-2. Non-metric (FRP) Reinforcement for Concrete Structures*, pp. 379–386, 1995.

[14] A. M. Mufti, B. M. Benmokrane, and k. J. Newhoo, "Durability of GFRP reinforced concrete in field structures," in *Proceedings of the 7th-FRPRCS,SP-23*, pp. 1361–1377, 2007.

[15] A. M. Mufti and J. Newhook, "Deformability versus ductility in concrete beams with FRP reinforcement," in *Proceedings of Adv. Composite Materials in Bridge and Structures*, pp. 189–199, 1996.

[16] X. Xing-sheng, *Research on Mechanical Property of FRP Bars and Flexural Property of Concrete Beams With FRP Bars*, Tianjing University, Tianjing, China, 2007.

[17] S. Peng-yong and J. Shi-yong, "Nonlinear finite element analysis on concrete beam reinforced with BFRP bars," *Concrete*, vol. 227, no. 9, pp. 33–35, 2008.

[18] L. Liang, "FRP reinforced concrete beam analysis and calculation of flexural capacity," *Sichuan Building Materials*, vol. 161, no. 37, pp. 45–49, 2011.

[19] Z. Hongjun, C. Haili, and J. Demin, *Special Concrete and New Concrete*, Chemical Industry Press, Beijing, China, 2004.

[20] Y. Choi and R. L. Yuan, "Experimental relationship between splitting tensile strength and compressive strength of GFRC and PFRC," *Cement and Concrete Research*, vol. 35, no. 8, pp. 1587–1591, 2005.

[21] G. Zhenhai and S. Xudong, *Theory and Analysis of Reinforced Concrete*, Tsinghua University Press, Beijing, China, 2005.

[22] M. Guijie and X. Huiqing, "Study on the uniaxial tensile performance of alkali-resistant glass fiber concrete," *Jilin Water Conservancy*, vol. 325, no. 6, pp. 39–41, 2009.

[23] G. B. Kim, K. Pilakoutas, and P. Waldron, "Finite element analysis of thin GFRC panels reinforced with FRP," *Construction and Building Materials*, vol. 23, no. 2, pp. 930–942, 2009.